INVESTIGATION OF THE CHARACTERISTICS OF HIGH-RESISTIVITY SILICA BASED HYBRID POROUS CORE PHOTONIC CRYSTAL FIBER FOR TERAHERTZ WAVE GUIDANCE

S. R. TAHHAN[a,*], A. J. GHAZAI[b], I. M. ALWAN[c], M. H. ALI[d]
[a] *Laser and Optoelectronic Engineering Department, College of Engineering, Al–Nahrain Universit,* Baghdad, Iraq,
[b]*Physics Department, College of Science, Al–Nahrain University, Baghdad, Iraq.*
[c]*Alhussain University College, Karbala, Iraq.*
[d]*Network Engineering Department, College of Engineering, Al-Iraqiya University, Baghdad, Iraq*

A porous core photonic crystal fiber (PC-PCF) is reported in this paper. The fiber comprises a hybrid core enclosed in a hexagonal cladding with high-resistivity float-zone silicon as the substrate material. Its effective material loss is 80% lower than bulk material absorption loss at an operating frequency of 1.0 terahertz (THz). Confinement loss in the order of 10^{-12} cm^{-1} and dispersion profile of 3.7 ± 0.15 ps/THz/cm within the range of 1.2 – 1.6 THz are attained under optimal parameters. Wave guiding properties, such as core power fraction, scattering loss and nonlinearity are also explored to further ensure the robustness of the proposed fiber. The proposed fiber has considerable potential in various short-distance THz applications, such as THz medical imaging, given its excellent guiding properties

(Received April 11, 2019; Accepted September 21, 2019)

Keywords: Terahertz, porous core photonic crystal fiber, PC-PCF, Effective material loss, High resistivity silica, HRS, Dispersion, Finite Element Method.

1. Introduction

The terahertz (THz) (10^{12} Hz) frequency window falls between the infrared and microwave bands of the electromagnetic spectrum and encompasses the frequency range of 0.1–10 THz. The security applications of THz technology have attracted attention because THz radiation penetrates fabrics and polymers [1]. In contrast to X-rays, THz radiation has low photon energies and is nonionizing; thus, it is used for accurate and harmless in vivo imaging [2]. Moreover, THz radiation has potential uses in high-speed long-range communications because its bandwidth is wider than microwave frequencies [3]. THz frequencies have strong resonances that stem from the vibrational and rotational transitions of a considerable number of molecular clusters and the transitions of various nanomaterials. Therefore, they are employed to probe spectroscopic emission/absorption spectra and shell structures in explosive sensing, weapons, DNA hybridization, biosensing, and drugs. Convenient waveguide solutions in the microwave and infrared regions have attracted research attention. Free space is the best medium for THz wave transmission in terms of low loss and low dispersion because dry air has the lowest absorption coefficient in the THz regime. Free-space propagation has several challenges, such as sender–receiver misalignment and path loss, which is influenced by the surrounding atmospheric conditions. Metallic [4] and dielectric waveguides [5] have also been used to transmit THz waves in addition to free space. Metallic waveguides, such as photonic crystal fibers (PCFs), face high Ohmic losses and have paved the way for advancements in the application of optical fibers as THz waveguides [6].

PCFs are a class of optical fibers that consist of morphological arrays of air holes stretching across the z-axis. PCFs for THz wave propagation are defined by the way they guide

* Corresponding author: shaymaa.riyadh@gmail.com

light. Light guidance by PCFs directly depends on the fiber's refractive index profile. Light is guided through the photonic bandgap or antiresonant effect if the core refractive index of the PCF is lower than that of the cladding. By contrast, light is guided through total internal reflection (TIR) when the core refractive index of the PCF is higher than that of the cladding. TIR-based THz PCFs consist of solid-material cores and present either regularly distributed dry air holes that span the cladding (solid core PCFs [SC-PCFs]) or regularly distributed dry air holes that span the finite expanse of the core and cladding (porous core PCFs [PC-PCFs]). SC-PCFs exhibit absorption losses and dispersion that are dependent on high frequencies; whereas PC-PCFs have low frequency absorption losses and dispersion given that dry air holes are distributed in their core regions. Several PC-PCFs have been proposed, and the majority of proposed PC-PCFs are constructed from polymer substrates [7]–[13]. These PC-PCFs, however, demonstrate high effective material losses (EMLs) that are attributable to the intrinsic absorption property of polymer materials. For example, the PC-PCFs recently proposed by [7]–[13] all have high EML values that are not less than 0.04 cm^{-1}. Most previous works did not discuss the bending loss property of PC-PCFs despite its importance for numerous THz applications in medical imaging [14].

The PC-PCF proposed in this work is constructed with HRS substrate. Few HRS-based PC-PCFs have been proposed in the past. A previous group [15] employed an epsilon near-zero material to induce birefringence in HRS-based fibers. This approach, however, may increase the fabrication complexity of PC-PCFs. The same group proposed another HRS-based PC-PCF with rectangular slots in the core [15]. Nevertheless, although noncircular core air holes may improve geometrical asymmetry, they make fiber fabrication more difficult. The present work aims to substantially reduce EML, improve power localization at core air holes, and curtail bending loss. Other important properties, such as effective area, nonlinearity and scattering loss, are also rigorously investigated to further ensure the robustness of the proposed fiber. HRS-based PC-PCFs that comprise a circular–star-shaped core combined with a compact conventional hexagonal lattice have never been reported in THz research.

2. Geometry

The physical geometry of the proposed structure, which consists of hexagonal cladding that surrounds a hybrid core, is shown in Fig. 1. A perfectly matched layer (PML), porous cladding, and porous core are located at the outermost, middle, and innermost regions of the proposed PC-PCF, respectively. The polymer materials used to design SC-PCFs are also applicable for the design of PC-PCFs. High-resistivity silicon is used as the background material of the proposed PC-PCF because its constant refractive index (n =3.417) is within 0.1–2 THz. The constant refractive index is crucial to minimizing material dispersion . Furthermore, HRS has an extremely low bulk absorption loss of 0.015 cm−1 at 1 THz [16]. Previous THz research has shown that HRS is the material with the highest transparency in THz frequencies. Several PC-PCFs that used HRS as the background material have been reported [15], [17].

A PML with a thickness of 10% of the total fiber radius is introduced to prevent the back-reflection of light onto the fiber. The PML is presented in Fig. 2, where the perfect electric conductor (PEC) and the perfect magnetic conductor (PMC) are depicted. The PEC ensures that the magnetic field is symmetric in the traverse direction while keeping the electric field asymmetric, whereas the PMC has an opposing function, that is, it ensures that the electric field is symmetric in the traverse direction while keeping the magnetic field asymmetric [18]. All cladding air holes have diameter d, and displacement is referred to as pitch, which is denoted by Λ. A hexagonal cladding structure is selected to compact the fiber to help improve the MTIR guidance. The air-filling fraction (AFF) is maintained at a constant value throughout iterative simulations. High AFF values would cause air holes to overlap and complicate fabrication. The core structure is designed within a circle with diameter $D_{core} = 2(\Lambda - d/2)$, where dc denotes the diameter of air holes. The hybrid structure consists of 31 air holes that are spaced with random intervals. A central air hole is surrounded by a circular lattice that comprises six air holes

.

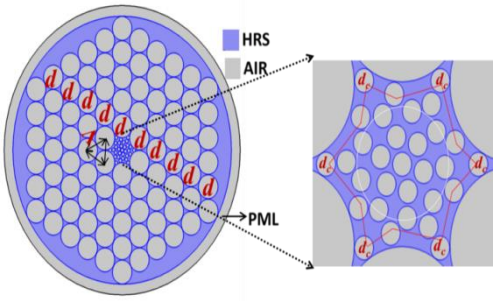

Fig. 1. Cross-section geometry of the proposed hybrid core fiber.

The third and fourth layers follow circular and star lattices, which are indicated by white and red lines, respectively. The hybrid lattice was selected to reduce the amount of material in the core and the overall production cost of the fiber. The finite element method is used to analyze the proposed PC-PCF shown in Fig. 2. The complete finer mesh consists 90,196 triangular elements, 8,212 boundary elements, and 492 vertex elements. The fiber has a total diameter and mesh area of 1.76 mm and 2,833,000 μm^2. The average element quality is 0.823. The mode field distribution of the proposed fiber with 75%, 80%, and 85% porosities at the operating frequency of 1 THz is given in Fig. 3. In this figure, the red arrows indicate the propagation direction. THz light is most and least localized at the core region with porosities of 75% and 85%, respectively.

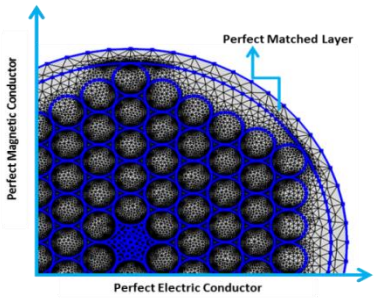

Fig. 2. Mesh of the proposed PCF under different boundary conditions.

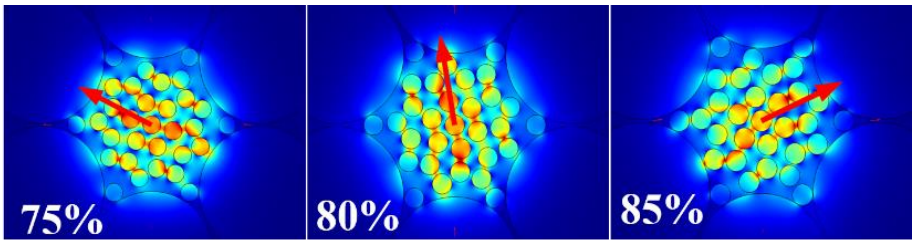

Fig. 3. Electric field distribution at Dcore = 160 µm; 85%, 80%, and 75% porosities; and 1 THz operating frequency.

3. Numerical method

Considering the loss properties of the PCF is important. EML and confinement losses are the main loss mechanisms. EML occurs when the bulk material absorbs incident THz light, and high EML values might affect the propagation length of the fiber. The EML αeff of the proposed hybrid fiber can be described by the following equation [7]:

$$\alpha_{eff} = \sqrt{\frac{\varepsilon_0}{\mu_0}}\left(\frac{\int_{mat} n_{mat}|E|^2 \alpha_{mat} dA}{2\int_{All} S_z dA}\right), cm^{-1}, \quad (1)$$

where ε_0 represents vacuum permittivity, $\mu 0$ represents vacuum permeability, n_{mat} represents the material refractive index, αmat is the bulk material absorption loss, and S_z represents the z component of the Poynting vector. $S_z = \frac{1}{2}Re|E \times H|$. E and H are the electric field and the complex conjugate of the magnetic field component, respectively. The numerator integral is computed over the bulk material region, whereas the denominator is integrated over the entire fiber cross-section.

Confinement loss (L_c) describes the degree of light localization at the core and depends on the optical density of the core region. Light tends to scatter across the cladding when confinement is high. Light scattering defeats the expected response of a PC-PCF. Confinement loss can be represented by the following equation [8]:

$$L_c = \left(\frac{4\pi f}{c}\right) Im(n_{eff}),\ cm^{-1}, \quad (2)$$

where *f* is modal frequency, *c* is the velocity of light, and $Im(n_{eff})$ is the imaginary part of the effective refractive index of the fundamental mode.

Combining Eqs. 1 and 2 provides the holistic loss of the fiber, which is popularly termed as total loss. Total loss provides considerable information on the fiber's loss behavior.

Core power fraction is another important property that describes the amount of power that propagates inside the hollow discontinuities of the core. It can be represented by the following equation [9]:

$$\eta' = \frac{\int_x S_z\, dA}{\int_{all} S_z\, dA} \times 100\ \%, \quad (3)$$

where S_z is the z component of the Poynting vector. Similar to EML enumeration, the numerator is integrated over the region of the core, whereas the denominator is evaluated for all fiber regions.

The effective core area is a quantification of the spatial extent of the fiber that is covered by the fundamental mode and can be mathematically represented by the following equation [13]:

$$A_{eff} = \frac{[\int I(r) r dr]^2}{[\int I^2(r) dr]^2}\ cm^{-1}, \quad (4)$$

where $I(r) = |E_t|^2$ is the transverse electric field intensity in the fiber cross-section.

Optical fibers routinely bend during application. Therefore, the bending extent of the fiber must be determined. The bending loss of the PCF is investigated by using the following analytical method [13], [19]:

$$\alpha_{BL} \approx \frac{1}{8}\sqrt{\frac{2\pi}{3}}\frac{1}{A_{eff}}\frac{1}{\beta} F\left[\frac{2}{3} R \frac{(\beta^2 - \beta_{cl}^2)^{\frac{3}{2}}}{\beta^2}\right], cm^{-1}, \quad (5)$$

where $F(x) = x^{-1/2} \exp(-x)$; R is the bending radius; and β is the propagation constant, which is $\beta = \frac{2\pi n_{eff}}{\lambda}$.

The collected power of the proposed PCF is determined by the numerical aperture (NA). It is a unit less parameter inversely proportional to the effective core area. NA is essential for noninvasive THz medical imaging applications and it is calculated by using the following [20];

$$NA = \frac{1}{\sqrt{1 + \frac{\pi A_{eff} f^2}{c^2}}} \quad (6)$$

The disproportionality between the hybrid core and the cladding air holes gives rise to high nonlinearity. The nonlinearity of the proposed fiber can be deduced using the following expression [20];

$$\gamma = \frac{2\pi}{\lambda} \times \frac{n_2}{A_{eff}} W^{-1}Km \tag{7}$$

where, n2 is the nonlinear coefficient of the core material and is m^2/W. For HRS, n_2= 3.51 x 10^{-12} cm^2W^{-1} in terahertz band [21]. Nonlinearity is crucial for several applications such as super continuum generation, optical signal, and high power applications.

The scattering loss arises due to the proposed fiber's geometrical inhomogeneity, light intensity and the deference in the material density. The scattering loss of the suggested fiber is calculated by the following equation [20];

$$\alpha_R = C_R \times \left(\frac{1}{\lambda}\right)^4 dB/Km \tag{8}$$

where, CR is the scattering coefficient of the background material ranging from 0.8×10^{-5} to 1.0×10^{-5} (dB/cm).(μm^4). The value of CR is chosen 1.0×10^{-5} (dB/cm) (μm^4) in this analysis.

The overall quality of the proposed PC-PCF in the THz regime can be assessed from the figure of merit (FOM). It is related to the effective area and the normalized effective material loss. FOM can be calculated using the following expression [22]:

$$FOM = \frac{\alpha_{eff}}{A_{eff}} \tag{9}$$

where, CR is the scattering coefficient of the background material ranging from 0.8×10^{-5} to 1.0×10^{-5} (dB/cm).(μm^4). The value of CR is chosen 1.0×10^{-5} (dB/cm) (μm^4) in this analysis.

THz sub pulses arrive at the receiver end at different times because they traverse the fiber with various speeds. This latency is known as pulse broadening and amounts to chromatic dispersion. However, chromatic dispersion is the sum of material and waveguide dispersions. Only waveguide dispersion is considered in this work because the HRS presents negligible material dispersion in THz frequencies. Waveguide dispersion mainly depends on geometric structure (e.g., size and position of air holes) and can be calculated with the following equation [12]:

$$\beta_2 = \frac{2}{c}\frac{dn_{eff}}{d\omega} + \frac{\omega}{c}\frac{d^2n_{eff}}{d\omega^2} \qquad ps/THz/cm, \tag{10}$$

where c is the speed of light in vacuum, neff is the effective refractive index, and $\omega = 2\pi f$ is the angular center frequency.

4. Parameter studies

As illustrated in Fig. 4, the impact of varying core diameter and porosity on the real part of the effective refractive index is investigated before loss properties are studied. The effective index increases with core diameter and decreases with porosity values because the core becomes occupied by additional HRS substrate as its size is increased. Furthermore, effective index decreases when porosity is increased because the HRS substrate is replaced with low-index dry air.

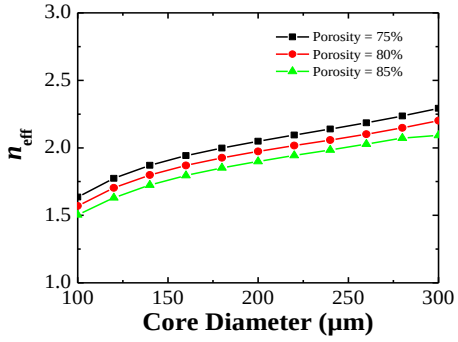

Fig. 4. EML versus core diameters at different core porosities and f = 1 THz.

EMLs as a function of core diameter at different core porosities are provided in Fig. 5. Material concentration in the core is determined by core diameter and porosity and is the main factor that causes high EMLs. High core porosity corresponds to low material concentration in the core and vice versa. EML linearly increases with core diameter for the same porosity values and decreases when porosity increases. This decrement is attributed to the substitution of solid HRS material with low-index air in the core.

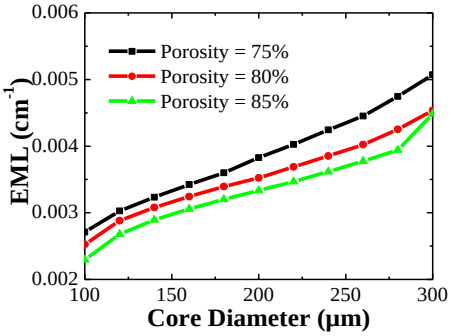

Fig. 5. EML versus core diameter at different core porosities and f =1 THz.

Confinement loss versus core diameter at porosities of 85%, 80%, and 70% is plotted in Fig. 6. Confinement loss exponentially decreases with the increment in core diameter at the same porosity and increases when porosity is increased because the increase in core diameter amounts to an increment in effective refractive index. This effect consequently broadens the core-cladding refractive index and strengthens mode field localization at the core. Confinement loss can be further reduced by increasing the number of air holes in the cladding region. This approach, however, increases fabrication complexity.

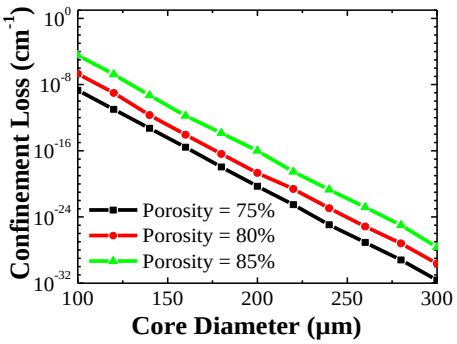

Fig. 6. Confinement losses versus core diameter at different porosities.

The summation of EML, confinement loss, and bending loss provides the total loss of the suggested PC-PCF. Total loss is governed by EML because confinement loss is negligible. The total loss of the PC-PCF versus frequency is illustrated in Fig. 7, wherein the behavior of the PC-PCF is similar to that of EML as shown in Fig. 4.

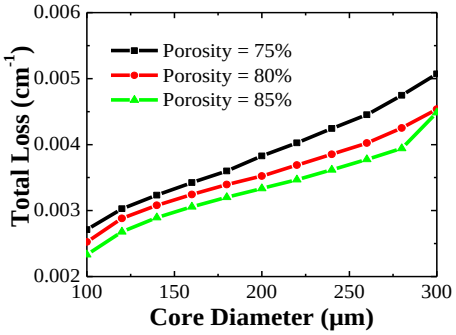

Fig. 7. Total loss versus core diameter at different porosities.

The relationship of the percentage fractional power flow in the core under the influence of the core diameter at different porosities is provided in Fig. 8. High porosity corresponds to high amounts of power flowing in core air holes as a result of the increased amount of dry air volume in the core. Dry air is the best medium for THz transmission. However, the decline in power fraction with the increase in core diameter may be attributed to the increase in EML at high core diameter values.

The highest core power fraction of 63.2% is obtained at a core diameter of 160 µm and porosity of 85%. The same set of core diameter and porosity values correspond to an ultralow EML of 0.003 cm−1 and a negligible confinement loss of 1.66 × 10−12 cm−1. Moreover, the total loss under the same parameter set is 0.003 cm−1. Therefore, the core diameter of 160 µm and porosity of 85% are selected as the optimal design parameters and shall form the basis of the rest of this work.

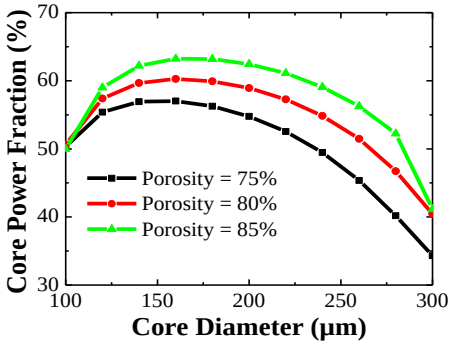

Fig. 8. Percentage core power fraction versus core diameter at different porosity values and f =1 THz.

The response of the real and imaginary parts of the effective refractive index to frequency is provided in Fig. 9. The real part increases as the imaginary part declines from 0.4 THz to 1.6 THz. The effective index is consistent with the relationship between frequency and electromagnetic phenomena. EML and confinement loss with respect to frequency at the core diameter of 160 µm and porosity of 85% are shown in Fig. 10.

EML increases with frequency as a result of the increase of incident electromagnetic waves. However, confinement loss decreases because of the increment in core-cladding index contrast stemming from the expansion of the index core region.

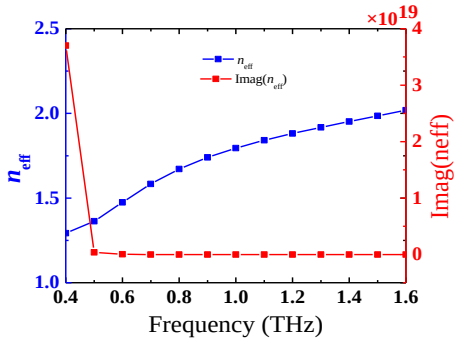

Fig. 9. Response of real and imaginary parts of the complex refractive index to source frequency.

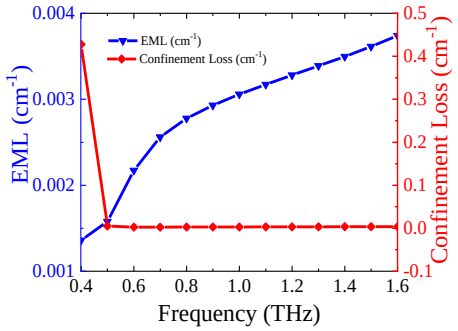

Fig. 10. EML and confinement loss versus frequency under 160 µm core diameter and 85% porosity.

The core power fraction and total loss with respect to frequency at the optimal core diameter of 160 µm and porosity of 85% are shown in Fig. 11. The core power fraction increases with frequency as a result of increasing the amount of incident electromagnetic waves [15]. Furthermore, total loss drastically reduces as frequency increases. The frequency of 1 THz is selected because it results in the highest fractional power flows in the core region, that is, 63.2%, at 85% porosity. The obtained core power fraction of the proposed PC-PCF is greater than that of previously reported PCFs at commensurate optimal parameters [7]–[9], [12], [13].

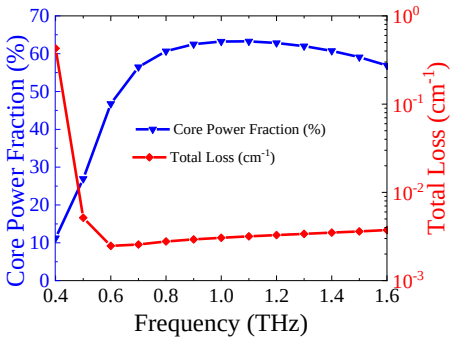

Fig. 11. Power fraction and total loss versus frequency under optimal design parameters.

Bending loss is provided as a function of core radius and frequency in Fig. 12. The figure shows that bending losses increase when the bend radius is small. The bending loss under the optimal porosity and core diameter values and 1 cm bend radius is 8.13×10^{-64} cm^{-1}. The effective

area and bending losses of the suggested PC-PCF agree with those of previously reported bend-insensitive THz waveguides [23], [24].

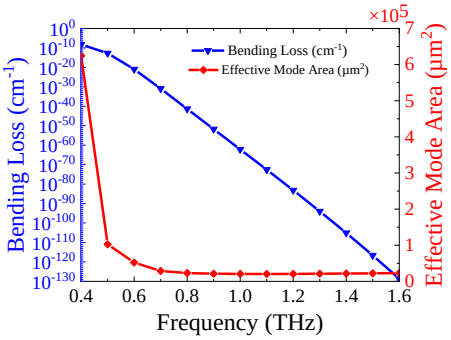

Fig. 12. Bending loss and effective area versus frequency at optimum design parameter and 1cm bend radius.

The dispersion profile is presented as a function of frequency under the optimal core diameter and porosity in Fig. 13 The hybrid PC-PCF shows a flattened dispersion of ±0.15 ps/THz/cm within a frequency range of 1.2–1.6 THz (500 GHz band). Moreover, the dispersion magnitude of the fiber at 1 THz is 4.89 ps/THz/cm. The obtained scattering loss of the proposed hybrid PC-PCF is presented in Fig. 14. The scattering loss increases with frequency due to increased intensity of light at high frequencies. Moreover, a negligibly low scattering loss of 1.24 × 10^{-12} dB/Km is obtained at 1 THz operating frequency.

The effective area, numerical aperture (NA), figure of merit (FOM) and nonlinearity of the proposed fiber are presented in Fig. 15.

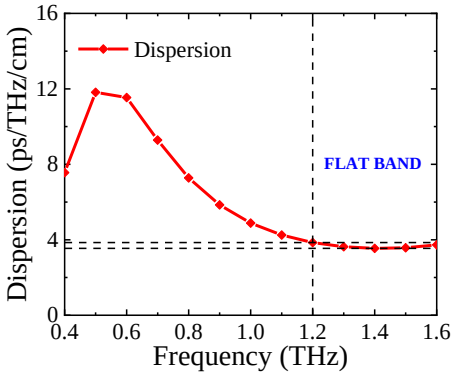

Fig. 13. Dispersion versus frequency for the proposed THz PCF.

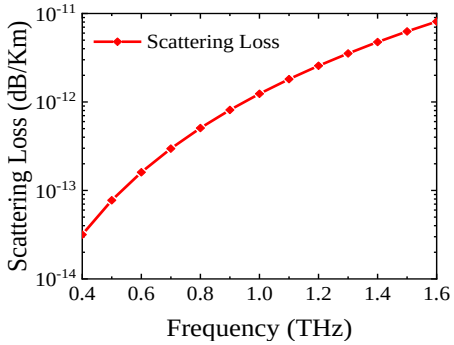

Fig.14. Scattering loss versus frequency for the proposed THz PCF.

The effective mode area increases with frequency under the optimal parameters. The area occupied by the fundamental mode reduces with the gradual increase in frequency. A high NA value of 0.76 is obtained at 1 THz operating frequency; the value makes the fiber potentially operable in various high power applications. The values of the nonlinearity and FOM at 1 THz are 0.35×10^{-7} $W^{-1}Km$ and 14×10^{-7} μm^2 respectively. Finally, the proposed fiber is compared with previously reported polymer and HRS-based PC-PCFs in Table 1. The proposed fiber is superior to previously reported PC-PCFs. For example, the reported total losses of the PC-PCF proposed in the present work is 70% and 65.52% lower than those of the HRS-based PC-PCFs proposed by [17] and [15], respectively.

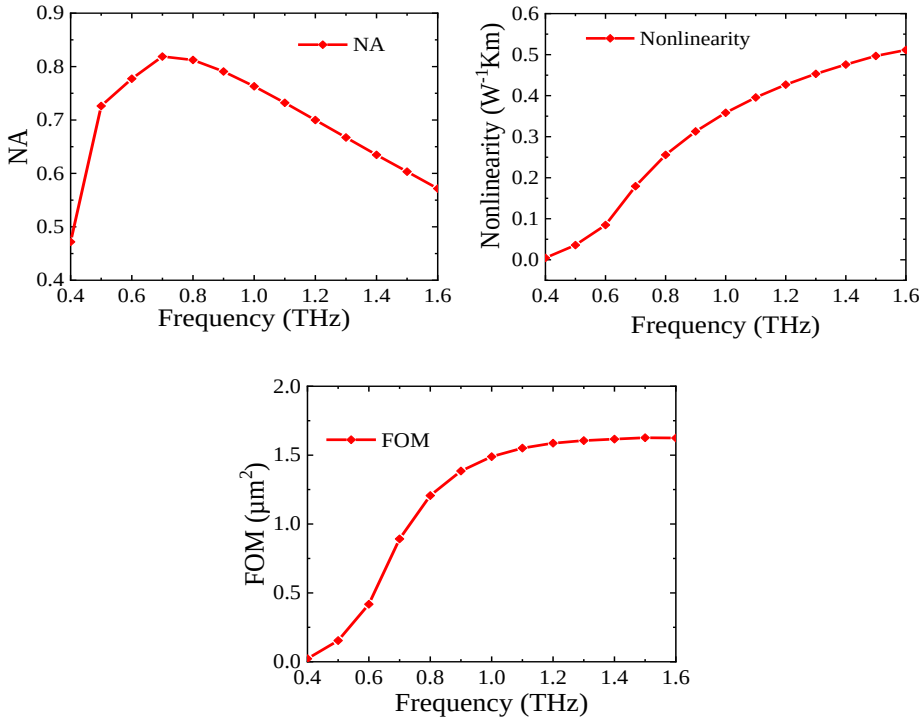

Fig. 15. Numerical aperture, nonlinearity FOM of the proposed fiber versus frequency.

Finally, the proposed fiber is compared with previously reported polymer and HRS-based PC-PCFs in Table 1. The proposed fiber is superior to previously reported PC-PCFs. For example, the reported total losses of the PC-PCF proposed in the present work is 70% and 65.52% lower than those of the HRS-based PC-PCFs proposed by [17] and [15], respectively.

Table 1. Comparison of the proposed PC-PCF with other existing PC-PCFs.

Ref	***Material***	***f*** **(THz)**	**EML** **(cm^{-1})**	**CL** **(cm^{-1})**	**BL** **(cm^{-1})**	**TL** **(cm^{-1})**	β_2 **(ps/THz/cm)**	**PF** **(%)**
[7]	Topas	1.00	0.081	10^{-5}	10^{-5}	-	±0.12	50
[8]	Zeonex	1.10	0.06	10^{-13}	-	-	±0.02	46
[9]	Topas	1.00	0.04	-	-	-	±0.1	50.4
[10]	Topas	1.00	0.0689	-	-	-	-	-
[11]	Zeonex	1.00	0.05	10^{-12}	-	10^{-12}	±0.38	67.05
[12]	Zeonex	1.00	0.07	10^{-3}	10^{-13}	-	±0.32	38
[13]	Topas	1.00	0.05	10^{-5}	10^{-6}	0.05	±0.06	40
[17]	HRS	1.00	-	-	-	0.01	-	-
[15]	HRS	1.00	0.0046	0.0041	-	0.0087	±0.5	-
[25]	Topas	1.00	0.0046	-	-	-	-	77
[22]	Topas	1.00	0.03	0.05	-	-	±0.2	47
This paper	HRS	1.00	0.003	10^{-12}	10^{-126}	0.003	±0.15	63.2

5. Conclusions

The physical and optical properties of a PC-PCF with a hybrid core and hexagonal cladding and constructed with high-resistivity silicon as the background material were thoroughly investigated. Under the optimal design parameters of 160 μm core diameter and 85% core porosity, the fiber demonstrated strong guiding property for THz waves with a total loss order of magnitude that was less than previously reported values. The fiber also has potential applications as a large-mode-area THz PCF given that it presented a large effective mode area of 20,532 μm^2.

It can be employed as a single-mode fiber with high transverse mode confinement at core air holes over a wide THz range at different core diameters and porosities. Its potential application can be expanded to THz communications because it obtained a flat dispersion variation of ±0.15 within a 500 GHz frequency band. Other important properties such as scattering loss, nonlinearity and figure of merit were also investigated. Finally, the hybrid PC-PCF can be easily fabricated given that its design is a complete departure from the designs of PC-PCFs with noncircular air holes.

References

[1] D. K. George and A. G. Markelz, "Terahertz Spectroscopy and Imaging," Springer, Berlin, Heidelberg, vol. 171, 2013.
[2] D. Crawley, C. Longbottom, V. P. Wallace, B. Cole, D. Arnone, and M. Pepper, J. Biomed. Opt. **8**(2), 303 (2003).
[3] S. Koenig et al., Nat. Photonics, 2013.
[4] M. Wächter, M. Nagel, and H. Kurz, Opt. Express, 2005.
[5] C. H. Lai, Y. C. Hsueh, H. W. Chen, Y. J. Huang, H. C. Chang, and C. K. Sun, Opt. Lett., 2009.
[6] S. Atakaramians, S. Afshar, T. M. Monro, and D. Abbott, Adv. Opt. Photonics **5**(2), 169 (2013).
[7] J. Luo et al., Appl. Opt., 2017.
[8] M. S. Islam et al., Appl. Opt., vol. 57, no. 4, p. 666, 2018.
[9] M. S. Islam, J. Sultana, J. Atai, D. Abbott, S. Rana, and M. R. Islam, Appl. Opt. **56(**4), 1232 (2017).
[10] K. Ahmed et al., Appl. Opt. **56**(12), (2017).
[11] J. Sultana, M. S. Islam, K. Ahmed, A. Dinovitser, B. W. H. Ng, and D. Abbott, Appl. Opt., 2018.
[12] M. A. Habib and M. S. Anower, Opt. Fiber Technol. **47**, 197 (2019).
[13] I. K. Yakasai, A. Rahman, P. E. Abas, and F. Begum, pp. 1–11, 2018.
[14] D. Grischkowsky, in Terahertz Biomedical Science and Technology, 2014.
[15] T. Yang, C. Ding, R. W. Ziolkowski, and Y. Jay Guo, J. Light. Technol., 2018.
[16] J. Dai, J. Zhang, W. Zhang, and D. Grischkowsky, J. Opt. Soc. Am. B, 2004.
[17] T. Yang, C. Ding, R. W. Ziolkowski, and Y. J. Guo, Opt. Express, 2018.
[18] W. C. Tay and E. L. Tan, J. Electromagn. Waves Appl., 2010.
[19] S. F. Kaijage, Z. Ouyang, and X. Jin, IEEE Photonics Technol. Lett. **25**(15), 1454 (2013).
[20] B. K. Paul, M. Golam Moctader, K. Ahmed, and M. Abdul Khalek, Results Phys., 2018.
[21] A. Woldegeorgis et al., J. Infrared, Millimeter, Terahertz Waves, 2018.
[22] B. K. Paul, M. S. Islam, S. Sen, K. Ahmed, and M. S. Uddin, Results Phys., 2018.
[23] M. R. Hasan, M. A. Islam, M. S. Anower, and S. M. A. Razzak, Appl. Opt. **55**(30), 8441 (2016).
[24] R. Islam, S. Rana, R. Ahmad, and S. F. Kaijage, IEEE Photonics Technol. Lett. **27**(21), 2242 (2015).
[25] N. Chen, J. Liang, and L. Ren, Appl. Opt., 2013.